Image simulation of projection systems in photolithography

P. Evanschitzky, T. Fühner and A. Erdmann
Fraunhofer Institute for Integrated Systems and Device Technology IISB
Schottkystrasse 10, 91058 Erlangen, Germany

ABSTRACT

The well-established Abbe formulation is one of today's most common approaches for the accurate image simulation of partial coherent projection systems used in semiconductor lithography. The development and application of lithographic imaging systems close to the theoretical resolution limits and the desire for the simulation of larger mask areas with high accuracy require several extensions of the classical Abbe approach.
This paper presents the basics of the Abbe approach including the so-called Hopkins assumption. For the accurate simulation of today's lithography systems important physical effects like strong off-axis illumination, small feature sizes, ultra-high NAs, a polarization dependent behavior, imaging demagnification, aberrations, apodizations, and Jones pupils have to be described and taken into account. The resulting extensions of the Abbe approach are presented. The accuracy, flexibility, and computational performance of the new approach are demonstrated by application examples.

Keywords: Lithography simulation, image simulation, image modeling, Abbe approach

1. INTRODUCTION

Lithography is one of the key steps in the fabrication of micro- and nanoelectronic circuits. It is used to transfer a designed pattern into a thin photosensitive polymer layer or photoresist on the top surface of a semiconductor wafer. The patterned photoresist serves as a mask for other process steps such as etching, implantation, and deposition. Serial writing techniques such as scanning with a focused optical or electron beam do not require a physical mask and can be used for the manufacturing of prototypes and masks for other lithographic techniques. However, the throughput of these serial techniques is too low for economical mass production in microelectronics. Parallel lithographic imaging techniques project an image of a physical mask into the photoresist on the semiconductor wafer. Advanced optical projection systems in semiconductor fabrication enable throughputs of more than 100 wafers per hour [1].
For more than 30 years optical projection lithography has been used as the standard technology for the patterning of microelectronic circuits. In the mid Seventies, systems with a wavelength of 436 nm were used to create patterns with a minimal feature size of 2000 nm. Nowadays, optical lithography at a wavelength of 193 nm is used to achieve a minimum feature size of 45 nm. This tendency to print features with sizes considerably smaller than the wavelength of the used light results in a tremendous increase of the complexity of lithographic processes. More and more physical and chemical effects have to be considered to understand and optimize the formation of images and photoresist profiles. The development of projection lithography for semiconductor fabrication has been accompanied by an improved understanding of the underlying physics and chemistry and by the development of predictive simulation tools. Nowadays, modeling and simulation of lithographic processes have become mandatory for the development and optimization of new processes [1].
Predictive simulation of lithographic processes requires the modeling of various physical and chemical phenomena. The light diffraction from sub-wavelength features on lithographic masks and wafers is governed by the system of Maxwell equations. Various electromagnetic field solvers are applied to solve relevant scattering problems. The accurate computation of image formation in high numerical aperture projection systems involves a plane wave decomposition of the scattered field, the application of appropriate transfer functions, and the accurate composition of the image-side fields according to their coherence and polarization properties. Standard transfer matrices from thin film theory are applied to describe the light propagation inside a homogeneous resist layer on the top of planar wafer stacks. The interaction of light and photoresist is characterized by a first order kinetics. The chemical modification of the exposed photoresist during a so-called post exposure bake is modeled by the numerical solution of a system of coupled kinetic- and diffusion equations. Finally, a combination of empirical development rate models and surface tracking algorithms such as the fast

marching method and cell removal methods is applied to describe the partial development of the photoresist. The resulting photoresist profile and its variation versus important process parameters are used for a quantitative characterization of lithographic processes [1].
Applications of lithography simulation range from training tools for researchers and engineers and comprehensive simulation studies to computational lithography for the design and optimization of new processes. Simple simulation sequences can be used to demonstrate the impact of different illuminations and mask geometries on the contrast of the resulting image. Lithography simulations are often used to explore new ideas and concepts before their actual implementation. Comprehensive parameter sensitivity studies are applied to investigate the impact of mask defects, optical aberrations, and other important factors on the lithographic performance and to support the definition of appropriate specifications for masks, lenses and other components of the lithographic system. Other types of simulation studies are focused on the comparisons of different lithography options such as double patterning/exposure, extreme ultra-violet (EUV) lithography, or immersion lithography with high index materials. Lithography simulation supports the optimization of bottom antireflective coatings (BARCs) which are used to improve the process stability of lithography over highly reflective substrates. Computational lithography, that is, the application of lithography simulation to a holistic optimization of lithographic processes, is considered to be one of the most important resolution enhancement technologies. Source/mask optimization (SMO) has demonstrated its potential to push 193 nm wavelength water immersion lithography with NA of 1.35 to the 22 nm technology generation [1].

2. SIMULATION MODELS

Lithography simulation typically involves two basic steps: Image formation and resist processing. Figure 1 shows schematically both steps. A mask with a design layout is projected into the photoresist. The left part of Figure 1 shows a mask layout defined by some dark features (the letters “IISB”, the width of the letter “I” is 32 nm) on a bright background. The projection of this mask on top of the photoresist (called aerial image) is shown in the middle left part of the figure. The second simulation step involves the modification of the photoresist chemistry and the geometry during baking steps and chemical development. Semi-empirical models are used to describe the concentration of important chemical species inside the resist and their impact on the solubility of the resist in the final development step. The resist profiles resulting from the projection of the mask into the resist with two different numerical apertures (NA) is shown in the middle right and right part of the figure. One can clearly see that the quality of the profile and in particular of details of the mask layout like lines (the letters “I”) and contact holes (inner parts of the letter “B”) strongly depend on the NA which is the most important parameter of the projection system. Beside the NA the image quality is mainly determined by the wavelength, direction, coherence and polarization of the illumination, by the defocus, and by the mask materials and geometry.

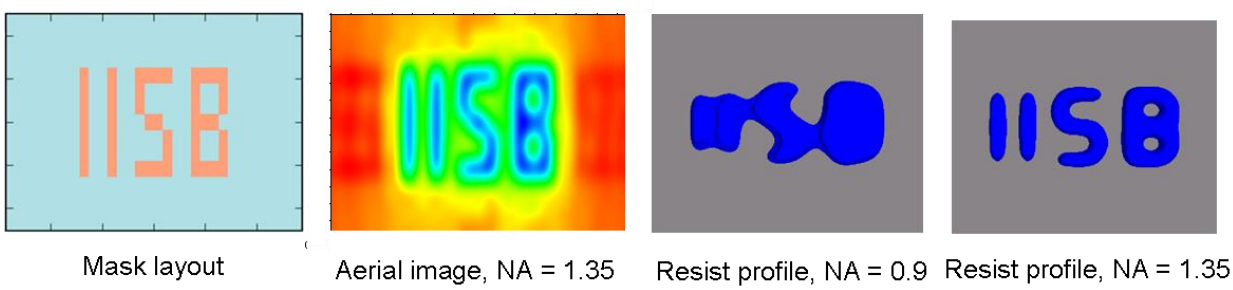

Figure 1: Mask layout (left), resulting aerial image with NA = 1.35 (middle left), resulting resist profile with NA = 0.9 (middle right) and with NA = 1.35 (right).

Figure 2 shows the basic configuration of a lithographic projection exposure. Advanced lithographic systems use an ArF excimer laser with an operating wavelength of 193 nm. Ultraclean water with a refractive index of 1.44 is used as immersion liquid. This provides numerical apertures up to 1.35. A 4× demagnification from the object (mask) to the image (wafer) plane alleviates the stringent requirements for accurate mask fabrication. The image formation inside the photoresist is impacted by refraction and reflection at the interfaces between immersion fluid, photoresist, and substrate. Bottom antireflective coatings (BARC) are used to reduce the negative impact of substrate reflections on the stability of the lithographic process [1].

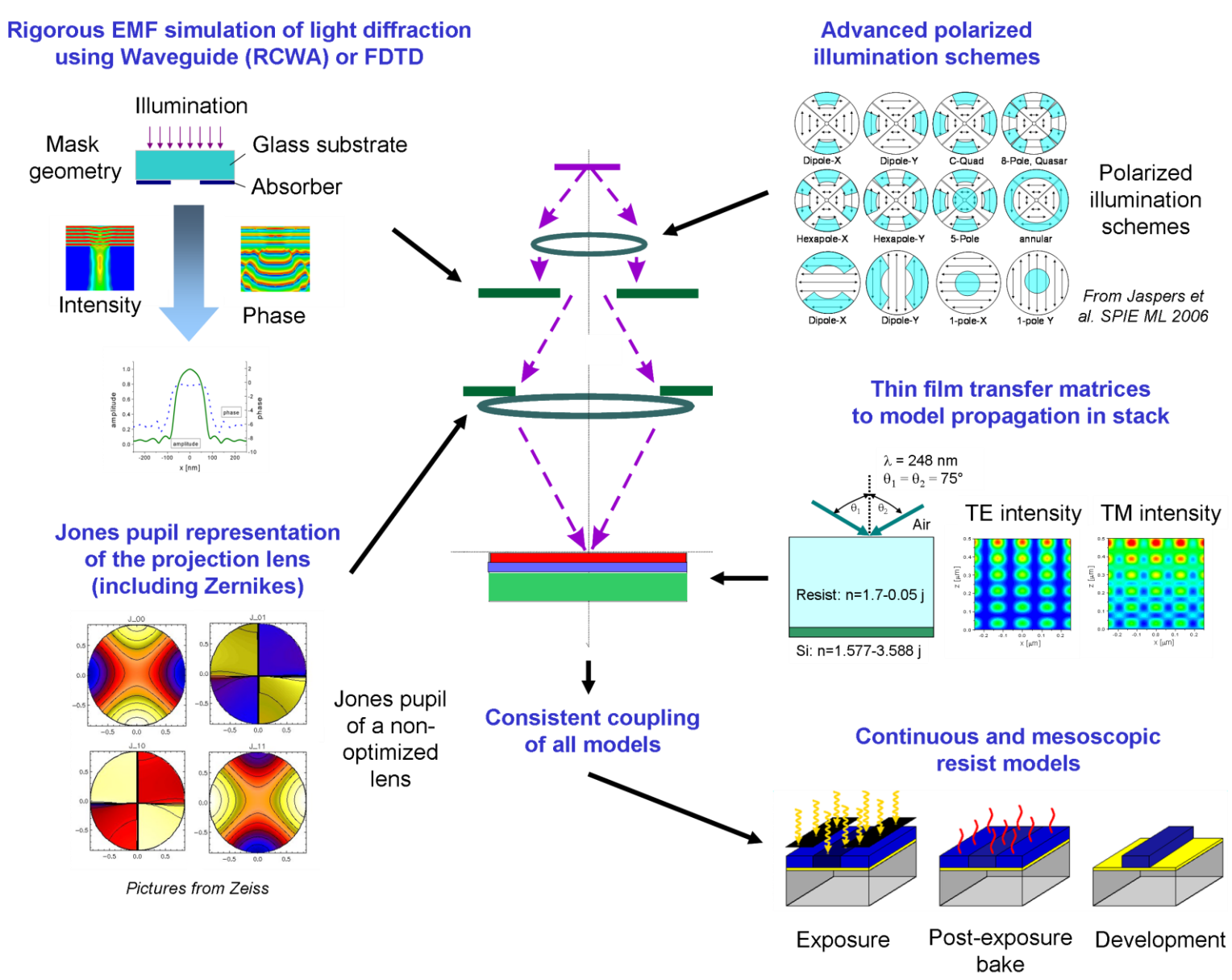

Figure 2: Basic setup of a lithographic projection exposure taking into account important physical effects required for an accurate simulation of advanced lithographic systems [2].

The accurate simulation of optical exposure involves several physical effects: A quasi-monochromatic light source with different geometries and polarization states (Figure 2 upper right part) is used to illuminate the mask. The patterns on the mask diffract the incident light. For the computation of the light diffraction a rigorous electromagnetic field (EMF) simulation has to be applied (Figure 2 upper left part). In case of relaxed feature sizes (e.g. 90 nm and larger) a simplified thin mask (Kirchhoff mask) model can be used. Depending on the NA the projection lens (lens system) collects a part of the diffracted light and directs it towards the photoresist/wafer to the image plane (Figure 2 central part). The light projection behavior of the real lens system (in contrast to an ideal lens system) is described by a so called Jones pupil and Zernike aberrations (Figure 2 lower left part). The light propagates into the wafer stack typically consisting of at least three different layers (substrate, bottom anti-reflective coating, and photoresist). For the computation a thin film transfer matrix model is used (Figure 2 middle right part). A consistent coupling of all described effects and models is required in order to guarantee a sufficiently high accuracy of the simulation results. Finally the light distribution inside the wafer stack is used for the following resist simulation which typically covers the three steps exposure, port-exposure bake, and development (Figure 2, lower right part).
In the following the image formation including all parts of Figure 2 except for the EMF simulation and the resist simulation will be described more in detail.

2.1 Image formation

The projection imaging of a mask can be considered as a bandpass filter. In general, partial coherent imaging is described by the Hopkins equation [3]. This equation involves a quadruple integral over a four-dimensional transmission factor, the so-called transmission coefficient (TCC). Two types of derivative algorithms of Hopkins's equation have been introduced: The so-called Abbe method [4] and a TCC decomposition into a sum of coherent systems (SOCS) [5]. In this paper, we focus on the Abbe algorithm which provides a physical interpretation of Hopkins's equation and is well adapted to accurate lithography simulations. The SOCS algorithm is preferred for the fast image calculation in optical proximity correction. The basic idea of the Abbe method can be expressed by the following equation 1 [1].

$$a(x,y) = F^{-1}\left[P(f_x,f_y)\cdot s(f_x-q_x,f_y-q_y)\right]$$
$$I_{tot}(x,y) = \sum_{Source} a(x,y)\cdot a^*(x,y) \qquad (1)$$

The projection lens covers a part of the diffracted light and transforms the corresponding Fourier components from the entrance pupil to the exit pupil. The image is obtained by the superposition of the band limited spectrum in the image plane.
Fourier transformation of the complex valued mask transmission provides the diffraction spectrum $s(f_x,f_y)$ of the mask in the far field at the entrance pupil of the projection lens. Depending on the mask geometry, feature sizes and materials and on the illumination wavelength, the mask transmission or the diffraction spectrum $s(f_x,f_y)$ have to be computed either with an EMF simulation or based on the simplified thin mask (Kirchhoff mask) model. In the next step the diffraction spectrum is shifted according to the illumination direction (q_x,q_y) of a specific source point and is then multiplied with the pupil function $P(f_x,f_y)$. This pupil function describes the impact of the projection lens (lens system) on the diffracted light (e.g. defocus, apodizations, wave aberrations). Diffraction orders outside the NA are not transmitted through the lens. Finally inverse Fourier transform (denoted by F^{-1}) of the transmitted spectrum produces a complex illumination source point dependent field a(x,y) in the image plane. The total image intensity $I_{tot}(x,y)$ is obtained by summation over all source points [1].

2.2 Extended Abbe approach

Increasingly aggressive characteristics of lithography systems like strong off-axis illumination, small feature sizes, ultra-high NAs, and a polarization dependent behavior, on the one hand and the desire for the simulation of larger mask areas with high accuracy and for increasingly complex simulation studies on the other hand, require several extensions of the classical Abbe approach. In order to achieve the required accuracy in combination with short simulation times, extensions of the physical model as well as optimizations of the simulation flow and of the mathematical computations have to be realized.
Most important, the fully vectorial spectrum of plane waves resulting from the diffraction of a given mask is accurately propagated through the imaging system. Therefore, a pupil sampling and a fit of the mask diffraction spectrum and of the pupil transfer function to the pupil sampling grid is not applied. In this new approach the vectorial pupil transfer function

of the projection lens is computed at the corresponding positions of the mask diffraction spectrum only. Since the Abbe approach is based on the image computation of single source points and incoherent superposition of the images of all source points a sampling is still required to represent typical source shapes by a finite number of source points. In order to realize a high accuracy and short simulation times, an appropriate selection of the points representing the source geometry is very important and implemented in the extended Abbe algorithm.
Figure 3 shows a schematic view of this new approach [6]. In the following description of the model the numbers in parentheses from (1) to (9) correspond to the numbers in the figure.

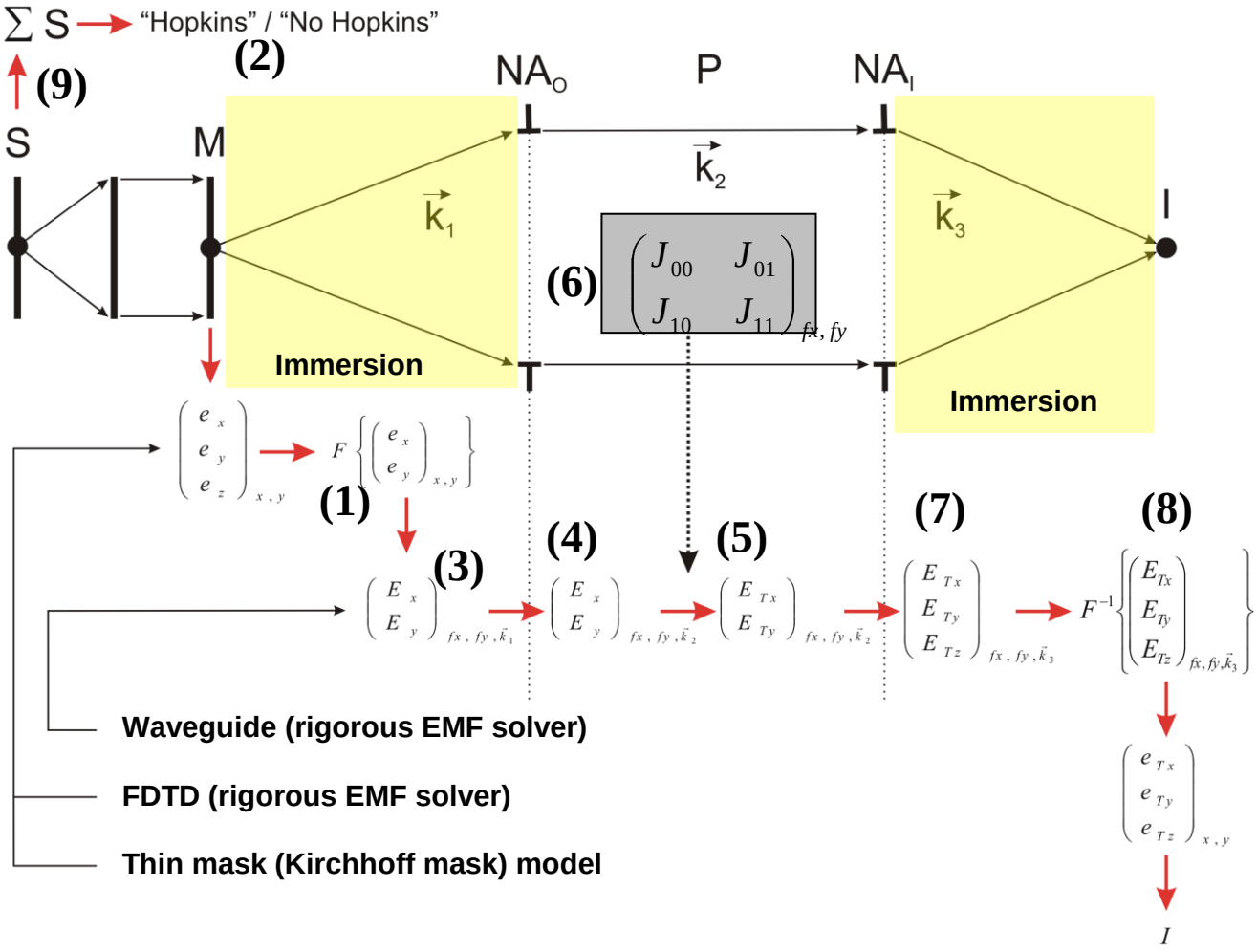

Figure 3: Schematic view of the extended Abbe model. The numbers in parentheses from (1) to (9) correspond to the numbers in the text. S is the illumination source, M is the mask, NA_O is the numerical aperture at the object side, P is the projector pupil, NA_I is the numerical aperture at the image side, I is the image, k_1, k_2, and k_3 denote the light propagation directions [6].

The simulation flow starts with the mask diffraction spectrum (1). This spectrum results from one source point illuminating the mask with a plane wave under a certain angle. In order to get the spectrum, two principle computation methods can be applied. A direct Fourier transformation of the mask geometry (thin mask/Kirchhoff mask model)

provides a reasonable approach of the mask diffraction spectrum. Accurate image modeling for advanced lithographic projection systems requires a rigorous computation of the diffracted light by an electromagnetic field solver like the finite difference time domain (FDTD) algorithm [7] or the Waveguide method [8]. In case of a rigorously computed mask spectrum either the "Hopkins" or the "No Hopkins" approach (2) can be applied [9]. In the first case only one rigorous computation, usually for the illumination point on the optical axis, is preformed. The diffraction spectra resulting from the other source points are determined by shifting the originally computed spectrum according to the illumination angle of the respective source point. In the second case (No Hopkins) the mask diffraction spectra are rigorously computed for several selected illumination source points. The number of rigorous computations is specified by the number of No Hopkins orders. The diffraction spectra of the remaining intermediate source points are obtained by interpolation.

A fully vectorial description of the mask spectrum is employed (3). This includes the consideration of different polarization states of source points like x- and y-polarized. Superposition of diffraction spectra of x- and y-polarized source points enables the simulation of arbitrary polarization states. The diffraction spectra are specified at spatial frequencies as given by the geometry of the mask. It is very important to note that no sampling is preformed at this point.

In the next step the mask diffraction spectrum is transformed from the mask plane to the pupil entrance plane and furthermore into the pupil (4) taking into account the required polarization and energy corrections. The pupil transfer function is applied to the spectrum (5). Therefore, the tensor-type function is computed at the spatial frequencies of the mask diffraction spectrum without any sampling of the pupil. This guarantees the highest possible accuracy and simulation speed. The pupil function can take into account basic features like NA, defocus, filters, polarizers, but also more complex properties like Jones data, and aberrations based on Zernikes (6). In the next step the spectrum is transformed from inside the pupil to the pupil exit plane (7) again taking into account high NA caused polarization and energy corrections. The intensity in the image plane is obtained by an inverse Fourier transformation of the spectrum at the exit pupil and superposition of all resulting components. For high simulation speed the inverse Fourier transformation is optimized by taking into account special physical properties of the image formation.

The described flow has to be repeated for all discrete source points. The superposition of the images resulting from the individual points (9) leads to the final aerial image. In order to realize a high accuracy and short simulation times an appropriate selection of points representing the source geometry is very important. A corresponding algorithm allowing arbitrary source shapes and polarization states is implemented in the extended Abbe algorithm.

Instead of computing an aerial image, the diffraction spectrum at the exit pupil can be coupled to a model based on the transfer matrix method (TMM). The TMM couples the diffraction spectrum to thin film transfer matrices. Inverse Fourier transformation for discrete layers provides the intensity distribution inside the photoresist or the full wafer stack (not shown in Figure 1), respectively. The individual layers result from user defined resolution of the stack in the direction of the optical axis. The same loop over all source point as described above must be performed. This coupling allows the computation of highly accurate bulk images for planar wafer stacks using the extended Abbe model.

3. APPLICATION EXAMPLES

3.1 Compensation of mask induced aberrations

The first example demonstrates the complexity of today's simulation applications and shows how the new imaging simulation approach can be used to solve such problems.

The rigorous simulation of light diffraction from optical and EUV masks in combination with the new extended Abbe based image simulation predicts mask induced phase effects with an aberration like impact on the imaging performance of lithographic projection systems. A significant best focus shift between different features can be observed. Since the overall focus budget is very limited a compensation of this effect is important. The goal of the simulation is to show that proper adjustment of the projector wavefront results in significant reduction of the best focus shift.

All simulations are done for 4× reduction water immersion lithography with a numerical aperture NA = 1.35 and a wavelength λ = 193 nm. The mask is a standard MoSi type attenuated phase shift mask (AttPSM). Simulations are done with unpolarized CQuad illumination with $\sigma_{in/out}$ = 0.7/0.9 and an opening angle of 20°. A 100 nm thick chemically amplified resist is deposited on a silicon wafer with a bottom antireflective coating. The wafer CD data are extracted at the bottom of the simulated profiles. The resist model parameters are obtained by calibration with experimental data [10]. Figure 4 presents simulated process windows of 60 nm contacts with pitches of 120 nm, 140 nm and 160 nm, respectively. A pronounced best focus difference for an aberration free imaging system between the dense and semi-dense contact arrays can be observed.

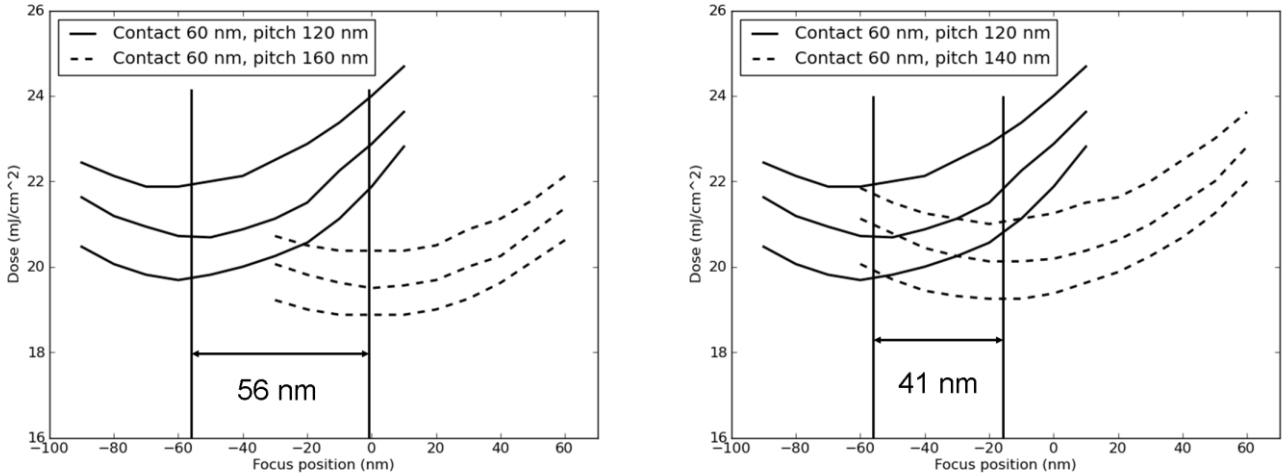

Figure 4: Process windows for contacts with different pitches. A pronounced best focus difference of 56 nm and 41 nm respectively between the dense and semi-dense contact arrays can be observed [10].

The application of projector wavefront control, e.g. as presented in [12], can compensate the effect. Figure 5 presents the computed maximum difference of the best focus positions (maximum best focus difference) for 60 nm contact arrays with five different pitches (120 nm, 130 nm, 140 nm, 150 nm, 160 nm) versus Zernike coefficients of the projector. Both first (Z_9) and second order (Z_{16}) spherical aberration show a pronounced minimum of the maximum best focus difference. The minima of third order and particularly of fourth order spherical aberration ($Z_{25,}$ Z_{36}) are less pronounced. The data in Figure 5 are obtained by application of individual Zernike terms. The question arises whether combinations of different Zernike terms can provide an additional reduction of the best focus shift for multiple pitches. Finding the best combination of multiple parameter scans would be very time consuming. Therefore, a genetic algorithm based optimization procedure using all simulation models shown in Figure 2 and 3 was developed to identify the best combination of Zernike terms.

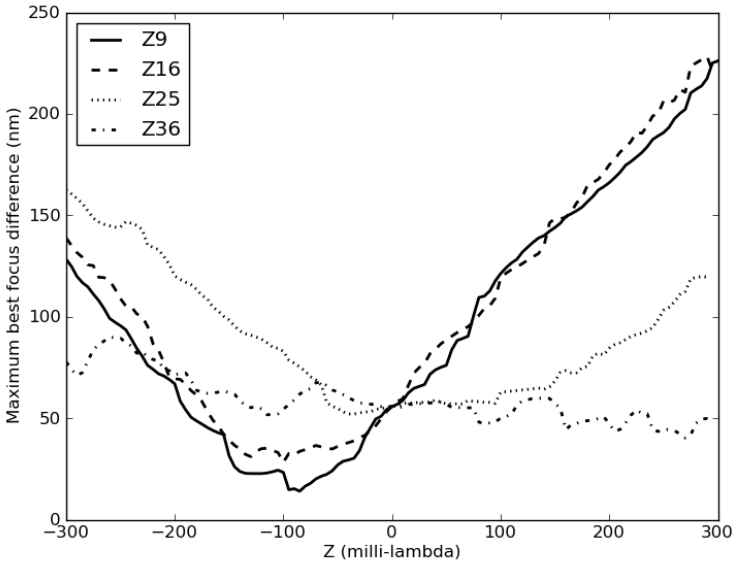

Figure 5: Maximum difference of the best focus positions for 60 nm contact arrays with five different pitches of 120 nm, 130 nm, 140 nm, 150 nm, and 160 nm versus projector Zernike coefficients Z_9, Z_{16}, Z_{25} and Z_{36} [10].

The optimization result for the 60 nm contacts with five pitches as mentioned above and five Zernike terms Z_4, Z_9, Z_{16}, Z_{25} and Z_{36} can be seen in Figure 6. In the figure only the two limiting process windows with the maximum best focus difference are shown. The process windows of the other pitches are in between.

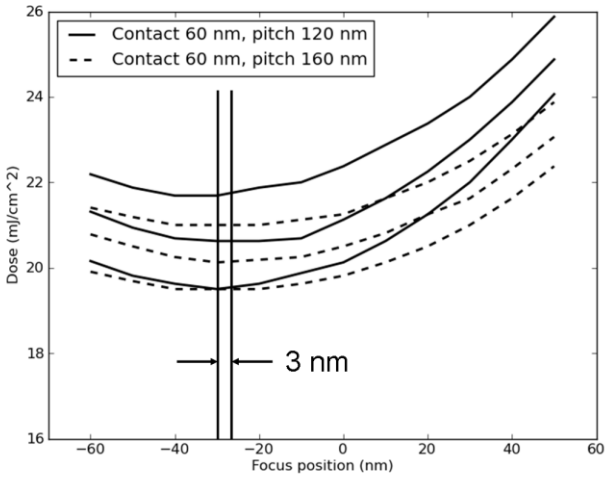

Figure 6: Process windows for contacts with different pitches. The maximum best focus difference between all pitches of 56 nm for a pupil without aberrations (shown in Figure 4 left) is reduced to 3 nm for a pupil with Z_4 = -7 mλ, Z_9 = -45 mλ, Z_{16} = -43 mλ, Z_{25} = 23 mλ and Z_{36} = 37 mλ. Only the two extreme process windows with the maximum best focus difference are shown [10].

The complex simulation scenario in this example requires a coupling of many different models and a huge number of individual highly accurate imaging simulations using the presented extended Abbe approach. The flexibility of the imaging model simplifies the definition of the corresponding simulations. Furthermore, due to the optimized imaging model according to section 2.2 an overall simulation time of only about two days on 16 CPUs (2.8 GHz) could be realized for more than 500000 individual imaging simulations and evaluations required for the final optimization shown in Figure 6.

3.2 Simulation of larger areas

Beside the simulation of individual features like lines and contacts the highly accurate simulation of larger mask areas with many different absorber structures becomes more and more important. This second example demonstrates the application of the new imaging approach to the simulation of such a larger area.

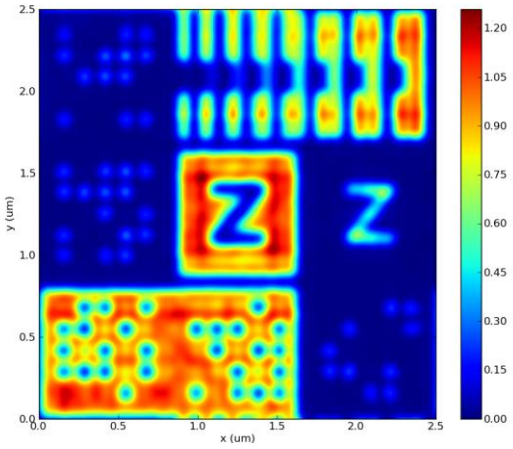

Figure 7: Aerial image of a 10 µm x 10 µm mask (size in mask scale) with different test structures. The image resolution is 1 nm. All models required for the accurate simulation of advanced lithography systems as described in Figure 2 and 3 are taken into account. The simulation time is only 9 seconds on one 2.8 GHz CPU.

Figure 7 shows the simulated aerial image of a 10 µm x 10 µm mask (size in mask scale) with several test structures. The mask is designed for accuracy comparisons between different simulation models. A state-of-the-art 193 nm immersion system with a NA of 1.35, a CQuad illumination, and a 4x reduction is assumed. The image is computed with a resolution of 1 nm. In order to guarantee the highest possible accuracy the extended Abbe approach including all models described in Figure 2 and 3 is used for the simulation.
Despite the highly accurate simulation of a larger mask area an aerial image simulation time of only 9 seconds on one 2.8 GHz CPU could be realized. This simulation time is still large compared to SOCS-type kernels which are used in OPC. However, the presented model does not require a pre-computation of kernels. The results are highly accurate and do not depend on the number of kernels which are considered in the image computation using SOCS.

3.3 EUV multilayer defects

The last simulation example demonstrates the application of the extended Abbe model to future simulation challenges. Exemplarily the simulation of an EUV multilayer defect is shown.
Defects below and inside the multilayer of an EUV mask belong to the most critical issues for EUV lithography. The defect induced deformation of the multilayer results in a local variation of the reflectivity which can have a significant impact on the printing result. Simulations are an essential tool for the investigation of the printing behavior of multilayer defects and for the development of defect compensation strategies. Figure 8 on the left shows the cross section of a defective EUV multilayer stack with an absorber on top of the stack. The defect on the bottom and the multilayer deformation can be seen. In the first step mask spectra for different positions of the defect with respect to the absorber are computed with the rigorous EMF solver Waveguide. In the next step the resulting aerial images are simulated with the extended Abbe model. Figure 8 in the middle and on the right show exemplarily the aerial images for two different defect positions. The black rectangles symbolize the absorber, the black arrows indicate the different multilayer defect positions. The significantly modified printing result of the absorber (dark blue area in both images) depending on the defect position can be seen clearly. For the simulations an EUV projection system with a NA of 0.3, a wavelength of 13.5 nm, and an unpolarized circular illumination with $\sigma = 0.52$ is assumed.

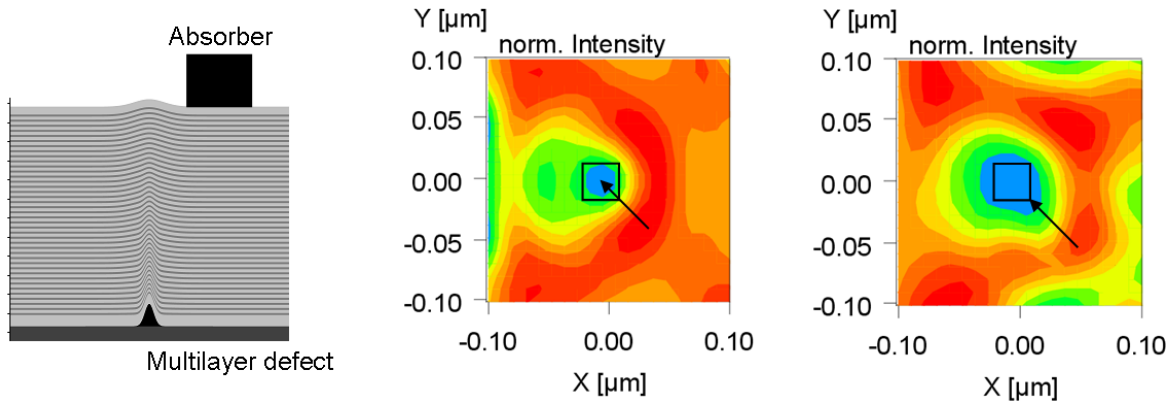

Figure 8: Cross section of a defective EUV multilayer with absorber (left), aerial image for the defect laterally placed below the absorber center (middle) and below the lower right absorber corner (right), the black rectangles symbolize the absorber, the black arrows show the different multilayer defect positions.

The extended Abbe imaging model and all other models used for the simulations in this paper are part of the lithography simulator Dr.LiTHO of Fraunhofer IISB [11]. Further simulation examples, accuracy and speed investigations, and comparisons with established simulation models can be found in [6].

4. CONCLUSIONS

In this paper a novel extended Abbe based imaging algorithm for fast and highly accurate simulations of current and future projection lithography systems is presented. The basics of lithography simulation and of the Abbe approach are

explained. For the accurate simulation of today's lithography systems important physical effects like strong off-axis illumination, small feature sizes, ultra-high NAs, a polarization dependent behavior, imaging demagnification, aberrations, apodizations, and Jones pupils have to be taken into account. This requires several important extensions of the classical Abbe approach. The resulting new approach is explained. Simulation examples demonstrate the accuracy, flexibility, and computational performance of the new approach.

REFERENCES

[1] Erdmann A., Fühner T., Shao F., and Evanschitzky P., "Lithography Simulation: Modeling Techniques and Selected Applications", Proc. SPIE 7390 (2009)

[2] From poster presented at SPIE AL, San Jose, CA, USA, 2011: Evanschitzky P., Shao F., Fühner T., and Erdmann A., "Compensation of mask induced aberrations by projector wavefront control", Proc. SPIE 7973 (2011)

[3] Hopkins H. H., "On the diffraction theory of optical image", Proc. R. Soc. London, Ser. A 217 408 (1953)

[4] Wong A. K. K., "Optical imaging in projection microlithography", SPIE Tutorial Text T66 (2005)

[5] Cobb N. B., "Fast optical and optical proximity correction in optical lithography and inspection", PhD thesis, University of Berkeley (1998)

[6] Evanschitzky P., Erdmann A., and Fühner T., „Extended Abbe approach for fast and accurate lithography imaging simulations", Proc. SPIE 7470 (2009)

[7] Erdmann A. and Friedrich C., "Rigorous diffraction analysis for future mask technology", Proc. SPIE 4000 (2000)

[8] Evanschitzky P. and Erdmann A., "Fast Near Field Simulation of Optical and EUV Masks Using the Waveguide Method", Proc. of SPIE 6533 (2007)

[9] Erdmann A., Citarella G., Evanschitzky P., Schermer H., Philipsen V., and De Bisschop P., "Validity of the Hopkins approximation in simulations of hyper-NA (NA>1) line-space structures for an attenuated PSM mask", Proc. SPIE 6154 (2006)

[10] Evanschitzky P., Shao F., Fühner T., and Erdmann A., "Compensation of mask induced aberrations by projector wavefront control", Proc. SPIE 7973 (2011)

[11] www.drlitho.com

[12] Finders J., Dusa M., Nikolsky P., van Dommelen Y., Watso R., Vandeweyer T., Beckaert J., Laenens B., and van Look L. "Litho and patterning challenges for memory and logic applications at the 22nm node", Proc. SPIE 7640 (2010)